Effect of the spin-orbit interaction on the band structure and conductance of quasi-one-dimensional systems

A. V. Moroz and C. H. W. Barnes
Cavendish Laboratory, University of Cambridge, Madingley Road, Cambridge CB3 0HE, United Kingdom
(Received 17 June 1999)

We discuss the effect of the spin-orbit interaction on the band structure, wave functions, and low temperature conductance of long quasi-one-dimensional electron systems patterned in two-dimensional electron gases (2DEG). Our model for these systems consists of a linear (Rashba) potential confinement in the direction perpendicular to the 2DEG and a parabolic confinement transverse to the 2DEG. We find that these two terms can significantly affect the band structure introducing a wave vector dependence to subband energies, producing additional subband minima, and inducing anticrossings between subbands. We discuss the origin of these effects in the symmetries of the subband wave functions. [S0163-1829(99)07143-X]

I. INTRODUCTION

In 1986, the first experimental realization of a quasi-one-dimensional electron system (Q1DES) in a dynamically confined two-dimensional electron gas (2DEG) was achieved.[1] Since then, there has been an extensive theoretical and experimental effort into understanding their basic properties (see, e.g., Refs. 2 and 3 and references therein). The interest in these systems stems from two facts. First, the effective transverse size of a Q1DES can be easily controlled and made remarkably small, down to the de Broglie wavelength of an electron. This makes it possible to realize experimental systems which have an arbitrary number of occupied transverse modes. Second, the high purity of 2DEG's grown by molecular beam epitaxy enables the almost collisionless motion of an electron through an experimental Q1DES. The coexistence of these two factors has made Q1DES unique objects for the investigation of transport phenomena yielding, in particular, the observation of the ballistic quantization of conductance[4,5] and the so-called 0.7 conductance structure.[6–8]

The process of electron transmission through a Q1DES involves the redistribution of incoming electron flux among its discrete eigenstates followed by adiabatic transport through them. Therefore, the determination of the electron eigenstates of a Q1DES is an integral and very important part of the more general quantum transport problem. This statement is especially relevant to the ballistic transport regime where the *total* conductance of a system is *completely defined* by the number of propagating electron modes which in turn can be uniquely calculated from the energy spectrum and the Fermi energy.[2,3,9]

Clearly, the energy spectrum of electrons crucially depends on the effective geometry of a Q1DES as well as on external and internal fields acting on them. Among the possible internal forces, one of the least understood examples is the interaction between orbital and spin degrees of freedom of an electron: the *spin-orbit interaction*, also referred to as the spin-orbit coupling. Although this interaction has an essentially relativistic nature (see, e.g., Refs. 10–12), it nevertheless can give rise to an observable modification of semiconductor band structure.[13–21]

A quite general theoretical approach to the description of the spin-orbit (SO) interaction is to use the following Hamiltonian,[10,11] which stems directly from the quadratic in v/c expansion of the Dirac equation:

$$\hat{H}_{SO}=\frac{\hbar}{(2M_0c)^2}\nabla V(\mathbf{r})(\hat{\boldsymbol{\sigma}}\times\hat{\mathbf{p}}). \tag{1}$$

Here, M_0 is the free electron mass, $\hat{\mathbf{p}}$ is the momentum operator, e is the elementary charge, $\hat{\boldsymbol{\sigma}}=\{\sigma_x,\sigma_y,\sigma_z\}$ is the vector of the Pauli matrices, $V(\mathbf{r})$ is the potential energy of the particle, and ∇ stands for the spatial gradient. The convenience (or universality) of the Hamiltonian (1) is that it does not restrict one to any particular form (model) of the potential $V(\mathbf{r})$, but allows freedom of choice depending on the nature and the symmetry of forces present in a given medium. Its form is such that it can remove the spin degeneracy in electron band structure while not actually producing an overall spin polarization.

In a bulk (3D) crystalline environment, the energy $V(\mathbf{r})$ arises exclusively from the periodic (microscopic) crystal potential. Most multicomponent semiconductors have either zinc-blende (GaAs and most III-V compounds) or wurtzite (II-VI compounds) lattice structure, both of which lack inversion symmetry. Dresselhaus[22] has shown that this property eventually leads to a SO-induced splitting of the conduction band into two subbands. The magnitude of the splitting is proportional to the cube of the electron wave number k.

In metal-oxide-semiconductor field effect transistors (MOSFET's) and heterostructures, the host crystals cannot be treated as ideal 3D systems, because the crystal symmetry is broken at the device interface where 2D electron or hole gases are dynamically confined in a quantum well. The reduction of the effective dimensionality lowers the symmetry of the underlying crystals and results in an additional (linear in k) term in the Dresselhaus splitting. Moreover, if the quantum well is sufficiently narrow, then the linear contribution is dominant[18,23–25] and, e.g., may reach $\sim$0.3–0.4 meV in 180-Å-thick modulation-doped GaAs wells.[18] Theoretical arguments[26] suggest that this can also be true in strained III-V crystals and hexagonal II-VI compounds.

Along with the *microscopic* crystal forces, there is another source of the potential energy $V(\mathbf{r})$ in 2D systems. It is caused by the interface electric field that accompanies the quantum-well asymmetry[3,27] and is directed along the normal to the device plane. Since the typical well width is $\sim 1-10$ nm, the interface potential turns out to be slowly varying on the scale of the lattice parameter and can be considered *macroscopic*, as opposed to the rapidly oscillating atomic field. The mechanism of the SO interaction originating from the interface field was first introduced by Rashba in Ref. 28. It also manifests itself as a linear in k splitting[29] of the 2D band structure. In a variety of systems including Si-MOSFET's,[30] InAs/GaSb,[23] and AlSb/InAs/AlSb (Ref. 20) quantum wells, $In_xGa_{1-x}As/In_xAl_{1-x}As$ heterostructures,[16,21] and GaAs electron gases,[31] it can be made to dominate the Dresselhaus terms, indicating the significance of macroscopic potentials in producing observable SO effects in low-dimensional systems.

In modern nanotechnology, there exists a number of methods for creating Q1DES from 2DEG's: the split-gate technique; wet and dry etching; and cleaved edge overgrowth.[32] In essence, they all exploit the confinement of the lateral (in-plane) motion of electrons (holes) by some transverse potential. Any such potential must be essentially nonuniform in space in order to force the charged particles to remain within a confined area. The spatial variation scale of the confining potential crucially depends on the particular fabrication method and varies over a wide range: $\sim 10-1000$ nm. Thus, in Q1DES one finds another example of macroscopic potentials, viz. the lateral confining potential, which is absent in higher-dimensional structures. The spatial nonuniformity of the confining potential gives rise to an additional (in-plane) electric field in the system. If the confinement is sufficiently strong (narrow and deep), then this field may not be negligible in comparison with the interface-induced (Rashba) field. Moreover, in nearly square (i.e., symmetric) quantum wells where the Rashba field is essentially suppressed,[20,31] the in-plane (''confining'') electric field is likely to be dominant. This suggests the possible importance of the lateral confining potential to the SO Hamiltonian (1) in Q1DES. We are not aware of any experimental evidence or measurement of the strength of the SO coupling resulting from such a confining potential and cannot therefore quote a grounded estimate for the corresponding energy modification. Nevertheless, the above arguments seem sufficiently strong to indicate a possible new mechanism for the SO interaction in Q1DES and point towards possible new transport effects. The existence of an additional (and easily controllable) source of the SO coupling could catalyze experiments on quantum-wire based devices that exploit both the charge and spin of an electron, e.g., spin transistors[33,34] and active spin polarizers.[35]

Our belief in the importance of the SO interaction in semiconductor Q1DES is strongly supported by the fact that observable manifestations of a SO-induced energy splitting have already been found experimentally[36] in another type of Q1DES, viz. in electron gases trapped by dislocational defects in silicon crystals. The source of the SO coupling in these systems is an electric field perpendicular to dislocations and the SO-related energy splitting is linear in the wave number k, which makes a physical analogy between the electron gas on dislocations and semiconductor Q1DES quite close. The SO interaction manifests itself in spin-dependent electron conductivity along dislocations which can be ascribed to combined spin resonance[28,37] of electrons corresponding to transitions between SO-split energy levels.

In this paper we analyze theoretically the effect of the spin-orbit interaction on the energy spectrum and conductance of a long Q1DES. As a model for the Q1DES, we use a strictly 2D electron gas subject to a transverse electrostatic confining potential. To decide on a reasonable shape of the confining potential, we assume a sufficiently small effective width ($\lesssim 300$ nm) for the Q1DES and a low electron concentration ($\lesssim 10^{11}$ cm^{-2}). Combined together, these two factors prevent the confining electric field from being significantly screened by the electron gas. Under these conditions, the confining potential can be accurately approximated by a parabolic potential.[38–40] This conclusion is very favorable to our problem because exact analytical expressions for the energy spectrum and wave functions of a 2D electron gas in a parabolic potential are well known and provide us with a good zero approximation in dealing with the SO coupling.

We include the SO interaction via the Hamiltonian (1). We assume that the potential $V(\mathbf{r})$ which is responsible for the SO coupling consists of two contributions: (i) a parabolic confining potential with a gradient (or the accompanying electric field) which lies in the plane of the 2DEG; (ii) a potential which arises from the asymmetry of the quantum well with the corresponding electric field (Rashba field) being uniform and directed perpendicular to the device plane. We neglect the crystal-field (Dresselhaus) contribution to $V(\mathbf{r})$.

The goal of this paper is to reveal the qualitative hallmarks of the SO interaction in Q1DES rather than to construct a complete and realistic spectral and transport theory. Therefore we use two major simplifications. First, we neglect the Coulomb interaction between electrons. At first sight one may not expect this approximation to work in low-concentration 2D electron systems where the Coulomb energy may exceed the kinetic energy by an order of magnitude. However, it has recently been shown theoretically[41] that the effect of electron-electron interactions on SO coupling in such systems can be plausibly taken into account via a renormalization of the SO coupling constant. More specifically, this renormalization leads to an enhancement (by 10–50%) of the strength of the SO interaction, which emphasizes the significance of the SO-related effects in low-dimensional electron systems. Our second simplification is the exploitation of one-band effective mass approximation[42] for the Schrödinger equation. Within this approximation, the influence of the crystal forces on electron dynamics in the conduction band is reduced to the renormalization of the electron mass and all interband transitions are left out. Despite the obvious simplicity, this approach works well[3,43] for a wide range of semiconductor materials.

Section II is the central part of the paper. It is devoted to the solution of the problem that we have outlined above and to the analysis of the results obtained. In Sec. II A we introduce the Hamiltonian of a 2DEG that includes the parabolic confining potential and the SO-interaction term (1). We take into account only those contributions to the SO Hamiltonian that arise from macroscopic (i.e., relatively smooth) poten-

tials, viz. from the quantum-well (Rashba) and the parabolic confining potentials. Since the operator (1) contains the Pauli matrices, we seek electron wave functions in the form of two-component spinors. Within such a representation, the Schrödinger equation turns out to be a system of two *coupled* differential equations with respect to the spinor components. In the next two subsections we solve this system for two physically different situations. Section II B deals with the case of zero Rashba SO coupling, where the entire SO interaction comes from the parabolic confining potential. Here the Schrödinger equations decouple and the electron wave functions and energy spectrum are found in an explicitly analytical form. In Sec. II C we consider a more general situation where both mechanisms of the SO-coupling are present. In this case we calculate the electron wave functions and energy spectrum numerically using the results of Sec. II B as a convenient basis. Afterwards, we analyze the energy spectrum obtained in order to reveal the basic features of both SO-coupling mechanisms. In Sec. II D we discuss possible manifestations of the SO interaction in the dependence of the ballistic conductance of a Q1DES on the Fermi energy. Section III summarizes the results of our research.

II. THEORY AND ANALYSIS

A. Problem statement. Spinor equation

Within one-band effective mass approximation[42] the Hamiltonian of a Q1DES can be written as

$$\hat{H}=\frac{\hat{\mathbf{p}}^2}{2M}+V_{LC}(\mathbf{r})+\hat{H}_{SO}, \tag{2}$$

where $\mathbf{r}=\{x,y\}$ is a 2D position vector and M is the effective electron mass. In line with Refs. 38–40, the *lateral confining potential* $V_{LC}(\mathbf{r})$ is approximated by a parabola

$$V_{LC}(\mathbf{r})=\frac{M\omega^2}{2}x^2. \tag{3}$$

The quantity ω controls the strength (curvature) of the confining potential. The in-plane electric field $\mathbf{E}_{LC}(\mathbf{r})$ associated with $V_{LC}(\mathbf{r})$ is given by $\mathbf{E}_{LC}(\mathbf{r})=-\nabla V_{LC}(\mathbf{r})=-M\omega^2\mathbf{x}$.

We assume that the SO interaction Hamiltonian $\hat{H}_{SO}$ (1) in Eq. (2) is formed by two contributions: $\hat{H}_{SO}=\hat{H}^{\alpha}_{SO}+\hat{H}^{\beta}_{SO}$. The first one, $\hat{H}^{\alpha}_{SO}$, arises from the asymmetry of the quantum well, i.e., from the Rashba mechanism[28,29] of the SO coupling. Since the interface-induced (Rashba) electric field can reasonably be assumed uniform and directed along the z axis, the term $\hat{H}^{\alpha}_{SO}$ can be described by the following expression:

$$\hat{H}^{\alpha}_{SO}=\frac{\alpha}{\hbar}(\hat{\boldsymbol{\sigma}}\times\hat{\mathbf{p}})_z=i\alpha\left(\sigma_y\frac{\partial}{\partial x}-\sigma_x\frac{\partial}{\partial y}\right). \tag{4}$$

The SO-coupling constant α takes values within a range $(1-10)\times10^{-10}$ eV cm for different systems.[16,21,23,29,31] For brevity, in what follows we will refer to the Rashba mechanism of the SO coupling as α coupling.

The second contribution $\hat{H}^{\beta}_{SO}$ to $\hat{H}_{SO}$ comes from the parabolic confining potential (3):

$$\hat{H}^{\beta}_{SO}=\frac{\beta}{\hbar}\frac{x}{l_\omega}(\hat{\boldsymbol{\sigma}}\times\hat{\mathbf{p}})_x=i\beta\frac{x}{l_\omega}\sigma_z\frac{\partial}{\partial y}. \tag{5}$$

Here, $l_\omega=(\hbar/M\omega)^{1/2}$ is the typical spatial scale associated with the potential V_{LC} (3). In Eq. (5) we have introduced the SO-coupling constant β. Comparison of typical electric fields originating from the quantum-well and lateral confining potentials allows one to conclude that a plausible estimate for β should be roughly 10% of α. Moreover, in square quantum wells where the value of α is considerably diminished[20,31] (by an order of magnitude) the constant β may well compete with α. Henceforth we adopt the term β coupling for the mechanism of the SO interaction arising from the lateral confining potential (3).

Our objective is to find eigenvalues and eigenfunctions of the Schrödinger equation $\hat{H}\Psi=E\Psi$ with the Hamiltonian $\hat{H}$ given by Eqs. (2)–(5). The wave function $\Psi=\Psi(\mathbf{r})=\{\Psi_\uparrow(\mathbf{r})\Psi_\downarrow(\mathbf{r})\}$ is a two-component spinor and the energy E is measured from the conduction band edge. It is easy to see that the Hamiltonian (2)–(5) is translationally invariant in the y direction. We therefore seek solutions to Schrödinger's equation in the form of plane waves propagating along the y axis, i.e., $\Psi_{\uparrow\downarrow}(\mathbf{r})=\exp(ik_y y)\Phi_{\uparrow\downarrow}(t)$. Here, $t=x/l_\omega$ is the dimensionless transverse coordinate, $\Phi_{\uparrow\downarrow}(t)$ is the transverse wave function, and k_y is the longitudinal wave number. After substituting this representation into the Schrödinger equation, we obtain a system of two differential equations with respect to the spinor components $\Phi_{\uparrow\downarrow}(t)$:

$$\Phi''_\uparrow+(\varepsilon_x-t^2+t_\beta t)\Phi_\uparrow(t)=(l_\omega/l_\alpha)[(k_y l_\omega)\Phi_\downarrow(t)+\Phi'_\downarrow], \tag{6}$$

$$\Phi''_\downarrow+(\varepsilon_x-t^2-t_\beta t)\Phi_\downarrow(t)=(l_\omega/l_\alpha)[(k_y l_\omega)\Phi_\uparrow(t)-\Phi'_\uparrow], \tag{7}$$

$$t_\beta=\frac{l_\omega}{l_\beta}(k_y l_\omega), \tag{8}$$

where $\varepsilon_x\equiv(k_x l_\omega)^2$ is the dimensionless transverse energy, $k_x^2=(2M/\hbar^2)E-k_y^2$, and the prime denotes a derivative with respect to t. The lengths l_α and l_β defined by

$$l_\alpha=\hbar^2/2M\alpha,\quad l_\beta=\hbar^2/2M\beta \tag{9}$$

are characteristic spatial scales associated with the α and β couplings, respectively. We note that the functions $\Phi_{\uparrow\downarrow}(t)$ depend on three dimensionless external parameters: l_ω/l_α, l_ω/l_β, and $k_y l_\omega$.

Equations (6) and (7) are arranged in such a way that all the terms which couple them together are collected on the right-hand side (rhs). It is interesting that this arrangement separates explicitly the α and β mechanisms of the SO interaction. Indeed, the α terms enter only the rhs, while all the β terms are contained on the lhs. This suggests that the β coupling is responsible for forming independent (''unperturbed'' or ''noninteracting'') wave functions $\Phi_{\uparrow\downarrow}(t)$, while the α coupling mixes them together to form the solution of the whole system (6) and (7).

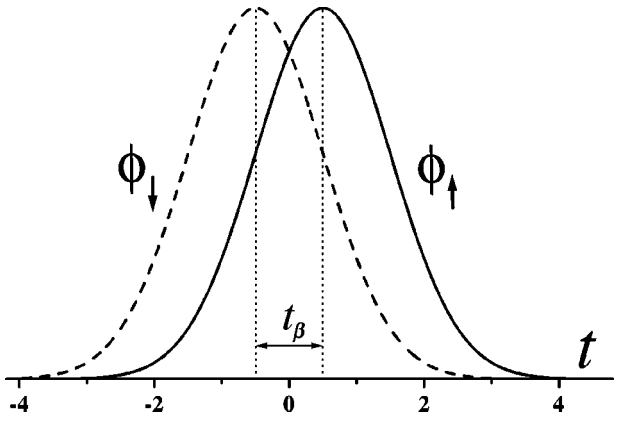

FIG. 1. The spinor components $\phi_\uparrow(t)$ and $\phi_\downarrow(t)$ for $n=0$, $l_\omega/l_\beta=0.1$, $l_\omega/l_\alpha=0.0$, $k_y l_\omega=10.0$.

B. Zero α coupling (square quantum well)

We start the analysis of Eqs. (6) and (7) with the situation in which the quantum well is square so that the interface-induced electric field vanishes. In terms of the SO interaction, this means that the Rashba mechanism (i.e., the α mechanism) of the SO coupling can be omitted. In other words, the characteristic length l_α of the α interaction tends to infinity: $l_\alpha\to\infty$, or $l_\omega/l_\alpha\to 0$. The study of this relatively simple case will provide us with a convenient basis for treating the general problem with finite l_α.

Once l_ω/l_α has been put equal to zero, the rhs in Eqs. (6) and (7) vanish and they transform into two independent Hermite equations[44] whose exact solutions are

$$\phi^n_{\uparrow\downarrow}(t)\equiv\Phi^n_{\uparrow\downarrow}(t)\big|_{l_\omega/l_\alpha=0}$$
$$=\frac{\exp[-(t\mp t_\beta/2)^2/2]}{\sqrt{2^n n!\,\pi^{1/2}}}H_n(t\mp t_\beta)\quad n=0,1,2,\ldots. \tag{10}$$

Here, $H_n(t)$ is the Hermite polynomial of nth order. The real wave functions $\phi^n_\uparrow(t)$ and $\phi^n_\downarrow(t)$ form complete sets with respect to the discrete quantum number n and are normalized by the following conditions:

$$\langle\phi^m_{\uparrow\downarrow}|\phi^n_{\uparrow\downarrow}\rangle\equiv\int_{-\infty}^{\infty}dt\;\phi^m_{\uparrow\downarrow}(t)\phi^n_{\uparrow\downarrow}(t)=\delta_{mn}, \tag{11}$$

where both $\phi^m_{\uparrow\downarrow}$ and $\phi^n_{\uparrow\downarrow}$ are taken at a same value of k_y.

From Eq. (10) one can see that the both ''up'' ($\phi^n_\uparrow$) and ''down'' ($\phi^n_\downarrow$) spinor components have exactly the same shape as functions of t but are spatially displaced with respect to each other by an amount of t_β (see Fig. 1). According to the definition (8), this displacement is a direct consequence of the β coupling because it does not vanish as long as $l_\omega/l_\beta\neq 0$ (except where $k_y l_\omega=0$). At finite values of t_β, the complete sets of functions $\phi^n_\uparrow(t)$ and $\phi^n_\downarrow(t)$ turn out *not* to be mutually orthogonal, i.e., $\langle\phi^m_{\uparrow\downarrow}|\phi^n_{\downarrow\uparrow}\rangle\neq\delta_{mn}$. Instead, the scalar cross product $\langle\phi^m_{\uparrow\downarrow}|\phi^n_{\downarrow\uparrow}\rangle$ in the case of sufficiently weak β coupling ($t_\beta\ll 1$) is governed by the following asymptotics:

$$\langle\phi^n_{\uparrow\downarrow}|\phi^n_{\downarrow\uparrow}\rangle=1-O(t_\beta^2), \tag{12}$$

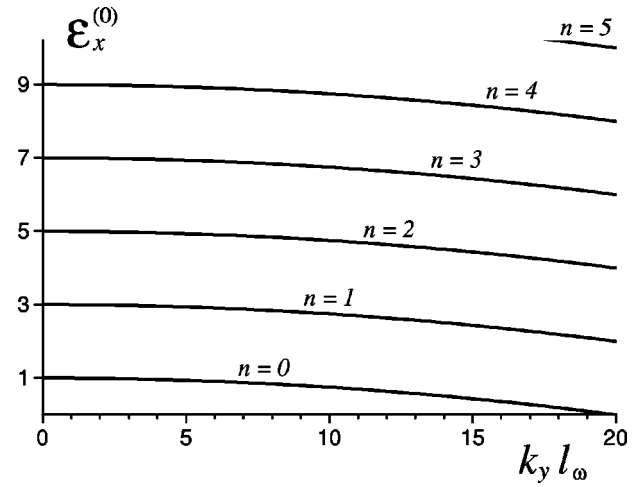

FIG. 2. The transverse energy $\varepsilon_x^{(0)}$ vs $k_y l_\omega$ for $l_\omega/l_\beta=0.1$.

$$\langle\phi^n_{\uparrow\downarrow}|\phi^{n+1}_{\downarrow\uparrow}\rangle\simeq\pm\sqrt{\frac{n+1}{2}}t_\beta=\pm\sqrt{\frac{n+1}{2}}\frac{l_\omega}{l_\beta}(k_y l_\omega), \tag{13}$$

$$\langle\phi^n_{\uparrow\downarrow}|\phi^{n-1}_{\downarrow\uparrow}\rangle\simeq\mp\sqrt{\frac{n}{2}}t_\beta=\mp\sqrt{\frac{n}{2}}\frac{l_\omega}{l_\beta}(k_y l_\omega), \tag{14}$$

$$\langle\phi^n_{\uparrow\downarrow}|\phi^{n\pm p}_{\downarrow\uparrow}\rangle=O(t_\beta^p)\quad\text{for}\quad p\geqslant 2. \tag{15}$$

The ''displacing effect'' of the β coupling on spinor wave functions [see Eq. 10 and Fig. 1] is superficially similar to the effect of a perpendicular magnetic field on a Q1DES. However, the essential difference is that a magnetic field shifts *both* spinor components $\phi^n_\uparrow(t)$ and $\phi^n_\downarrow(t)$ *as a whole* by an amount proportional to the strength of the magnetic field (see, e.g., Ref. 11), but it does *not* affect their *mutual* spatial distribution. In contrast to this, as can be seen in Fig. 1, the β coupling causes a spatial separation of the spin-polarized electron states $\phi^n_\uparrow(t)$ and $\phi^n_\downarrow(t)$.

Although the β coupling shifts the spinor components $\phi^n_{\uparrow\downarrow}(t)$ apart, it nevertheless is not capable of lifting their energy degeneracy. The dimensionless transverse energy $\varepsilon_x^{(0)}$ corresponding to the both eigenfunctions $\phi^n_{\uparrow\downarrow}(t)$ (10) is given by (see Fig. 2)

$$\varepsilon_x^{(0)}\equiv\varepsilon_x^{(0)}(n,k_y)=2n+1-(t_\beta/2)^2$$
$$=2n+1-\frac{1}{4}\left(\frac{l_\omega}{l_\beta}\right)^2(k_y l_\omega)^2. \tag{16}$$

The total electron energy E then forms parabolic subbands for each nth transverse mode:

$$E\equiv E_n(k_y)=\frac{\hbar\omega}{2}\varepsilon_x^{(0)}(n,k_y)+\frac{\hbar^2k_y^2}{2M}. \tag{17}$$

For zero β coupling ($l_\omega/l_\beta=0$) formulas (16) and (17) describe the well-known electric subbands.[9,10]

C. Finite α coupling (triangular quantum well)

We now examine the situation where the effective geometry of the quantum well is such that the interface-induced

electric field is nonzero. An example is the triangular well which forms at a heterojunction interface.[3,27] This interface-induced field gives rise to a finite α coupling and therefore to finite values of the coupling constant l_ω/l_α. For arbitrary nonzero values of l_ω/l_α, eigenvalues of Eqs. (6) and (7) cannot be obtained as simply as they were in the case of $l_\omega/l_\alpha=0$. To analyze the energy spectrum in the presence of α coupling, we will follow the scheme proposed in Ref. 45. Namely, we first expand the unknown functions $\Phi_{\uparrow\downarrow}(t)$ in terms of the unperturbed solutions $\phi_{\uparrow\downarrow}(t)$ (10) of Eqs. (6) and (7):

$$\Phi_{\uparrow\downarrow}(t)=\sum_{m=0}^{\infty} f_{\uparrow\downarrow}^m \phi_\uparrow^m(t), \tag{18}$$

$$\Phi_{\uparrow\downarrow}(t)=\sum_{m=0}^{\infty} g_{\uparrow\downarrow}^m \phi_\downarrow^m(t). \tag{19}$$

We then substitute the expansions (18) and (19) into Eqs. (6) and (7), respectively, and make use of the property[44]

$$\frac{d}{dt}\phi_{\uparrow\downarrow}^n(t)=\sqrt{\frac{n}{2}}\phi_{\uparrow\downarrow}^{n-1}(t)-\sqrt{\frac{n+1}{2}}\phi_{\uparrow\downarrow}^{n+1}(t) \tag{20}$$

to remove the derivative with respect to t on the rhs of Eqs. (6) and (7). We next multiply the equations obtained by $\phi_\uparrow^n(t)$ and $\phi_\downarrow^n(t)$, respectively, and integrate them over t from $-\infty$ to ∞. Owing to the orthogonality condition (11), the summation over m is removed by the δ symbol δ_{mn} and we find the simple vector relations:

$$\mathbf{f}_\uparrow=\hat{U}_\uparrow\mathbf{f}_\downarrow, \tag{21}$$

$$\mathbf{g}_\downarrow=\hat{U}_\downarrow\mathbf{g}_\uparrow. \tag{22}$$

Here, $\mathbf{f}_{\uparrow\downarrow}\equiv\{f_{\uparrow\downarrow}^0,f_{\uparrow\downarrow}^1,\ldots,f_{\uparrow\downarrow}^n,\ldots\}$ and $\mathbf{g}_{\uparrow\downarrow}\equiv\{g_{\uparrow\downarrow}^0,g_{\uparrow\downarrow}^1,\ldots,g_{\uparrow\downarrow}^n,\ldots\}$ are vectorized coefficients of the expansions (18) and (19), respectively, and $\hat{U}_{\uparrow\downarrow}$ are tridiagonal matrices defined by their elements:

$$U_{\uparrow\downarrow}^{nn}=\frac{l_\omega}{l_\alpha}\frac{k_y l_\omega}{\varepsilon_x-\varepsilon_x^{(0)}(n)}, \tag{23}$$

$$U_{\uparrow\downarrow}^{n,n+1}=\pm\frac{l_\omega}{l_\alpha}\left(\frac{n+1}{2}\right)^{1/2}\frac{1}{\varepsilon_x-\varepsilon_x^{(0)}(n)}, \tag{24}$$

$$U_{\uparrow\downarrow}^{n+1,n}=\mp\frac{l_\omega}{l_\alpha}\left(\frac{n+1}{2}\right)^{1/2}\frac{1}{\varepsilon_x-\varepsilon_x^{(0)}(n+1)}. \tag{25}$$

Note that the matrices $\hat{U}_{\uparrow\downarrow}$ are neither symmetric nor antisymmetric.

Equations (21)–(25) illustrate the effectiveness of the representations (18) and (19). Indeed, by using the functions $\phi_{\uparrow\downarrow}^m(t)$ as expansion bases, we have reduced differential operators on the lhs of Eqs. (6) and (7) to the scalar factor $\varepsilon_x-\varepsilon_x^{(0)}(n)$. In other words, matrices which were supposed to act on $\mathbf{f}_\uparrow$ and $\mathbf{g}_\downarrow$ in Eqs. (21) and (22) turn out to be diagonal within the representations (18) and (19).

Our next step is to find the relationship between the vectors $\mathbf{f}_{\uparrow\downarrow}$ and $\mathbf{g}_{\uparrow\downarrow}$. To do this, we equate the rhs of Eq. (18) to that of Eq. (19) and take the scalar product of the resulting equation with $\phi_\uparrow^n(t)$. After making use of the orthogonalization condition (11), we find that

$$\mathbf{f}_{\uparrow\downarrow}=\hat{W}_\uparrow\mathbf{g}_{\uparrow\downarrow}, \tag{26}$$

where the matrix $\hat{W}_\uparrow$ is defined by

$$W_{\uparrow\downarrow}^{mn}=\langle\phi_{\uparrow\downarrow}^m|\phi_{\downarrow\uparrow}^n\rangle. \tag{27}$$

According to Eq. (10) [see also Eqs. (12)–(15)] the matrices $\hat{W}_{\uparrow\downarrow}$ are *not* diagonal as long as the β coupling is *finite*.

Analogously, by taking a scalar product of the rhs of Eqs. (18) and (19) by $\phi_\downarrow^n(t)$, it can be shown that

$$\mathbf{g}_{\uparrow\downarrow}=\hat{W}_\downarrow\mathbf{f}_{\uparrow\downarrow}. \tag{28}$$

Finally, we combine relations (21), (22), (26), and (28) into a closed homogeneous equation with respect to $\mathbf{f}_\uparrow$: $\mathbf{f}_\uparrow=\hat{U}_\uparrow\hat{W}_\uparrow\hat{U}_\downarrow\hat{W}_\downarrow\mathbf{f}_\uparrow$. In order for this equation to have a nontrivial solution, the Jacobian matrix must satisfy the following condition:

$$\det(1-\hat{U}_\uparrow\hat{W}_\uparrow\hat{U}_\downarrow\hat{W}_\downarrow)=0. \tag{29}$$

The roots ε_x of this equation determine the dispersion law of electrons (see, e.g., Ref. 45). Here, $\varepsilon_x\to\varepsilon_x^{(0)}$ as $l_\omega/l_\alpha\to0$.

Alternatively, the relations (21), (22), (26), and (28) could have been resolved with respect to $\mathbf{g}_\downarrow$, which would have led to the permuted Jacobian matrix $\hat{U}_\downarrow\hat{W}_\downarrow\hat{U}_\uparrow\hat{W}_\uparrow$. However, such a permutation leaves the determinant unchanged and therefore the dispersion equation (29) would have been still applicable.

To obtain the solution of Eq. (29) for given values of the external parameters l_ω/l_α, l_ω/l_β, and $k_y l_\omega$, we truncated the infinite matrix $1-\hat{U}_\uparrow\hat{W}_\uparrow\hat{U}_\downarrow\hat{W}_\downarrow$ down to the first N rows and columns and used a numerical root finder to obtain the zeros of its determinant. Owing to the conveniently chosen bases (18) and (19), the roots of Eq. (29) converge very quickly to their exact values as N is increased. For instance, for l_ω/l_α, $l_\omega/l_\beta\lesssim1$, it suffices to take $N\approx30$ to find the ten lowest energy levels with a net error $<10^{-8}$.

The energy spectrum $\varepsilon_x=\varepsilon_x(k_y l_\omega)$ calculated by this procedure is shown in Fig. 3. Let us first consider the case of negligibly weak β coupling, when $l_\omega/l_\beta\to0$ [Fig. 3(a)]. Here we see twofold spin degeneracy of all quantum levels at $k_y=0$. As soon as we move away from the point $k_y=0$, the SO interaction lifts the degeneracy and produces an energy splitting $\Delta_R=\varepsilon_x^\uparrow-\varepsilon_x^\downarrow$ proportional to k_y, where $\varepsilon_x^{\uparrow\downarrow}$ are energies associated with the ''up'' and ''down'' spin polarizations, respectively. This linear behavior agrees with both theoretical predictions[41,28,29,45] and experimental observations[16,20,21,23] of the Rashba splitting in 2D systems.

The linear dependence of Δ_R on k_y can be easily deduced analytically from Eqs. (6) and (7) within first-order perturbation theory with respect to the parameter l_ω/l_α. Indeed, if we treat the rhs of Eqs. (6) and (7) as perturbations, then the first-order correction $\Delta\varepsilon_x^{\uparrow\downarrow}=\varepsilon_x^{\uparrow\downarrow}-\varepsilon_x^{(0)}$ to the unperturbed energy (16) will be given by

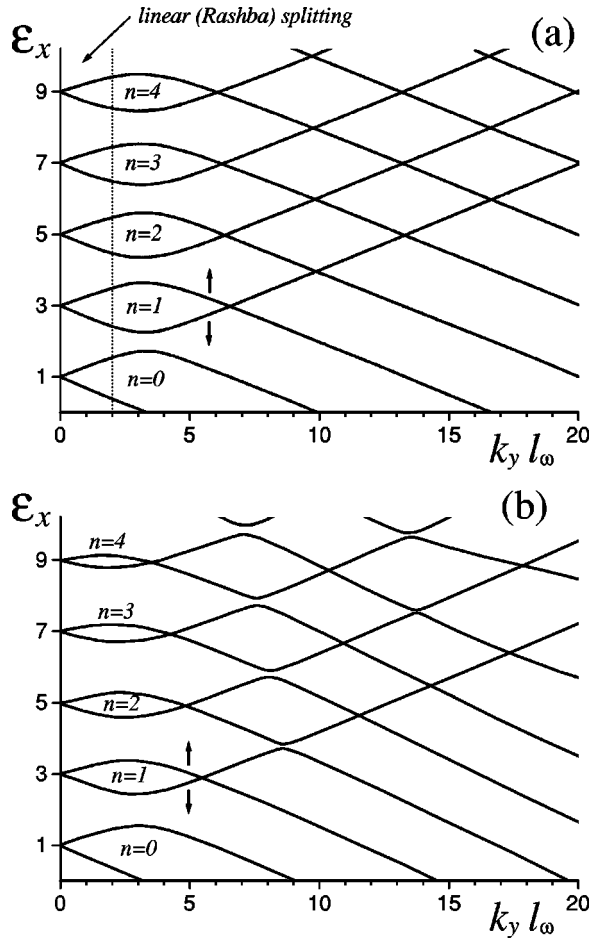

FIG. 3. The transverse energy ε_x vs $k_y l_\omega$ for finite α coupling ($l_\omega/l_\alpha=0.3$): (a) $l_\omega/l_\beta=0$; (b) $l_\omega/l_\beta=0.1$.

$$\Delta\varepsilon_x^{\uparrow\downarrow}\simeq\pm\sqrt{\hat{P}_\uparrow^{nn}\hat{P}_\downarrow^{nn}}, \tag{30}$$

or

$$\Delta_R=\varepsilon_x^{\uparrow}-\varepsilon_x^{\downarrow}\simeq 2\sqrt{P_\uparrow^{nn}P_\downarrow^{nn}}. \tag{31}$$

Here, $P_{\uparrow\downarrow}^{nn}$ are diagonal matrix elements of perturbation operators $\hat{P}_{\uparrow\downarrow}$:

$$P_{\uparrow\downarrow}^{mn}\equiv\langle\phi_{\uparrow\downarrow}^m|\hat{P}_{\uparrow\downarrow}|\phi_{\downarrow\uparrow}^n\rangle, \tag{32}$$

$$\hat{P}_{\uparrow\downarrow}=\frac{l_\omega}{l_\alpha}\left(\pm\frac{d}{dt}+k_y l_\omega\right). \tag{33}$$

To calculate the matrix elements $P_{\uparrow\downarrow}^{nn}$ we use the property (20) and take into account that

$$\langle\phi_{\uparrow\downarrow}^m|\phi_{\downarrow\uparrow}^n\rangle=\delta_{mn}\quad\text{for}\quad l_\omega/l_\beta=0 \tag{34}$$

[see Eqs. (12)–(15)]. As a result, we obtain

$$P_{\uparrow\downarrow}^{nn}\simeq(l_\omega/l_\alpha)(k_y l_\omega)$$

and hence the Rashba splitting Δ_R (31) is governed by

$$\Delta_R\simeq 2\frac{l_\omega}{l_\alpha}(k_y l_\omega)\quad\text{for}\quad l_\omega/l_\beta=0, \tag{35}$$

i.e., it is indeed proportional to the longitudinal wave number k_y.

The perturbative result (35) applies as long as $\Delta_R\ll\varepsilon_x^{(0)}(n+1)-\varepsilon_x^{(0)}(n)$, i.e., if $(l_\omega/l_\alpha)(k_y l_\omega)\ll 1$. For $l_\omega/l_\alpha=0.3$ this condition restricts $k_y l_\omega$ to values much less than about 3. In Fig. 3(a) we see that the linear behavior of the energy splitting for all the curves holds true until $k_y l_\omega\approx 2$ (dotted line). Within the region $k_y l_\omega\lesssim 2$, the asymptotic (35) gives a very good fit to all the energy branches. However, as soon as $k_y l_\omega$ becomes larger than ≈ 2.5, the dispersion curves start to bend. Eventually, this leads to an *anticrossing* of branches corresponding to quantum levels with neighboring discrete numbers n. This fact drastically contrasts the simpler situation with no confining potential (3), where the linearly split spectrum (35) represents the exact solution.[29]

Usually[11] anticrossing is associated with similar symmetry (''hybridization'') of underlying states (wave functions). To reveal possible symmetries in our case, we return to the perturbation theory with respect to l_ω/l_α and consider first-order corrections $\delta\Phi_{\uparrow\downarrow}^n(t)$ to the wave functions (10):

$$\delta\Phi_{\uparrow\downarrow}^n(t)=\sum_{m\neq n}\frac{P_{\uparrow\downarrow}^{mn}}{\varepsilon_x^{(0)}(n)-\varepsilon_x^{(0)}(m)}\phi_{\uparrow\downarrow}^m(t). \tag{36}$$

Owing to the orthogonality condition (34) the second (constant) term in Eq. (33) does *not* contribute to $\delta\Phi_{\uparrow\downarrow}^n(t)$ (36) for any $m\neq n$. At the same time, according to Eqs. (20) and (34), the first (differential) term in Eq. (33) gives rise to *nonzero* matrix elements P_{mn} for $m=n+1$ and $m=n-1$. As a result, $\delta\Phi_{\uparrow\downarrow}^n(t)$ (36) takes the form:

$$\delta\Phi_{\uparrow\downarrow}^n(t)\simeq\pm\frac{1}{2\sqrt{2}}\frac{l_\omega}{l_\alpha}\{\sqrt{n}\,\phi_{\uparrow\downarrow}^{n-1}(t)+\sqrt{n+1}\,\phi_{\uparrow\downarrow}^{n+1}(t)\}\quad\text{for}\quad l_\omega/l_\beta\to 0. \tag{37}$$

The total (perturbed) wave function is given by $\Phi_{\uparrow\downarrow}^n=\phi_{\uparrow\downarrow}^n+\delta\Phi_{\uparrow\downarrow}^n$. Figure 4 shows graphs of $\Phi_{\uparrow\downarrow}^n(t)$ for $n=0$ and $n=1$.

Equation (37) demonstrates that the nth quantum state is no longer independent of its ''neighbors,'' i.e., of the $(n\pm 1)$-st states. In turn, the $(n+1)$-st state now depends on its own nearest neighbors, i.e., on both the nth and the $(n+2)$-nd states. Owing to this interstate coupling, all spinors Φ^n partially acquire the symmetry properties of spinors $\Phi^{n\pm 1}$. Moreover, since the result (37) is perturbative, it is plausible that the interstate coupling becomes more pronounced when the perturbative approach breaks down, i.e., when $k_y l_\omega\gtrsim 2.5$. This ''hybridization'' of electron states accounts for the anticrossing of neighboring energy branches in Fig. 3(a).

After passing the relatively narrow anticrossing region $2.5\lesssim k_y l_\omega\lesssim 4.5$, all the curves in Fig. 3(a) straighten out and adopt a very accurate linear behavior for $k_y l_\omega\gtrsim 5$. There are two main features that attract attention in the infinite interval $k_y l_\omega\gtrsim 5$: (i) there are no further anticrossings of approaching energy branches. Even those with closest quantum numbers n, which anticrossed at smaller values of $k_y l_\omega$, now cross; (ii) all the straight lines $\varepsilon_x^{\uparrow\downarrow}(n)$ go down (up) with the same slope $\approx\mp l_\omega/l_\alpha$ which is independent of a level number n.

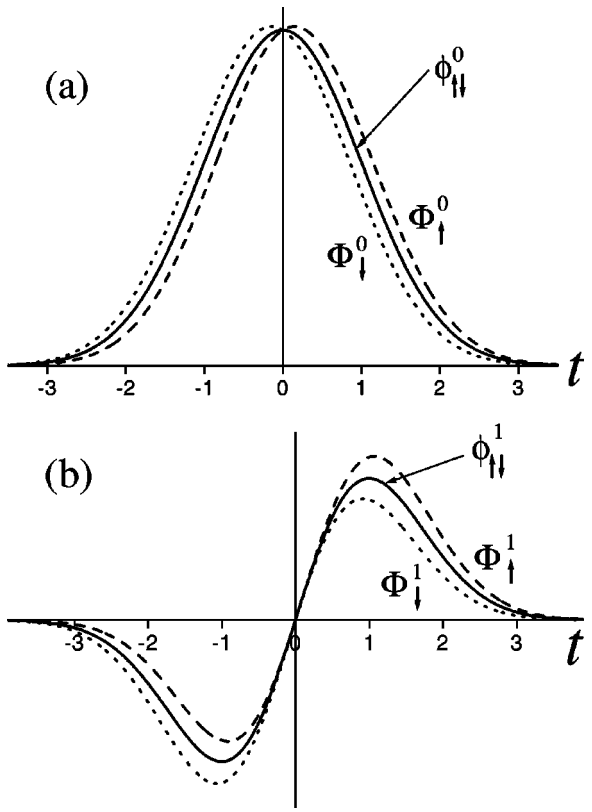

FIG. 4. Unperturbed wave functions ($l_\omega/l_\alpha=0$, solid curve) and wave functions modified by the α coupling ($l_\omega/l_\alpha=0.3$, the dashed curve describes the ''up'' and the dotted curve the ''down'' spin orientations): (a) $n=0$; (b) $n=1$. Zero β coupling ($l_\omega/l_\beta=0$) is assumed. For definiteness, we take $k_y l_\omega=0$.

Although statement (i) means asymptotical smallness (rather than absolute absence) of anticrossings in the region of large $k_y l_\omega \gtrsim 5$ in Fig. 3(a), these anticrossings are much weaker than any other anticrossings in the system and therefore can be left out.

To explain these properties we should return to Eqs. (6), (7), and (10). According to Eq. (10), the spatial variation scale of functions $\phi^n_{\uparrow\downarrow}(t)$ is of the order unity. This means that the derivatives $\Phi'_{\downarrow\uparrow}$ on the rhs of Eqs. (6) and (7), respectively, can be roughly estimated as $\Phi_{\downarrow\uparrow}$, at least for $|t| \lesssim 1$ and sufficiently small values of l_ω/l_α. Hence, it seems plausible that within the region, where $k_y l_\omega \gg 1$, the terms $\Phi'_{\downarrow\uparrow}$ can be neglected in comparison with $(k_y l_\omega)\Phi_{\downarrow\uparrow}$. Taking this into account together with the condition $l_\omega/l_\beta=0$, we reduce Eqs. (6) and (7) to

$$\Phi''_{\uparrow}+(\varepsilon_x-t^2)\Phi_{\uparrow}(t)=(l_\omega/l_\alpha)(k_y l_\omega)\Phi_{\downarrow}(t), \tag{38}$$

$$\Phi''_{\downarrow}+(\varepsilon_x-t^2)\Phi_{\downarrow}(t)=(l_\omega/l_\alpha)(k_y l_\omega)\Phi_{\uparrow}(t). \tag{39}$$

Unlike the general problem (6) and (7), Eqs. (38) and (39) can be simply decoupled by a unitary transformation in the spin space. The corresponding matrix has the form

$$\begin{pmatrix} 1/\sqrt{2} & -1/\sqrt{2} \\ 1/\sqrt{2} & 1/\sqrt{2} \end{pmatrix}. \tag{40}$$

It is straightforward to verify that eigenvalues (energies) of the decoupled equations are

$$\varepsilon_x^{\uparrow\downarrow}=2n+1\mp(l_\omega/l_\alpha)(k_y l_\omega), \tag{41}$$

and eigenfunctions are identical to those given by Eq. (10) at $l_\omega/l_\beta=0$. The formula (41) yields the expected linear dependence of both $\varepsilon_x^{\uparrow}$ and $\varepsilon_x^{\downarrow}$ on $k_y l_\omega$ with slopes $\mp(l_\omega/l_\alpha)$ independent of a level number n. The asymptotics (41) give a very accurate fit to the spectral pattern in the region $k_y l_\omega \gtrsim 5$ in Fig. 3(a). Since Eqs. (38) and (39) can be decoupled by a simple rotation, states $\Phi^n_{\uparrow}$ and $\Phi^n_{\downarrow}$ turn out to be intrinsically independent of each other as well as of all the other states. This fact alone explains why the anticrossing of energy branches is not observed for sufficiently large values of $k_y l_\omega$.

Let us now consider how the energy spectrum is modified by switching on the β coupling [Fig. 3(b)]. From visual comparison of Figs. 3(a) and (b) we see that the main effect of the β coupling is to *enhance* considerably the anticrossing of ''neighboring'' spectrum branches. Moreover, the strength of the anticrossing now depends on the quantum number n and grows as n is increased. An interesting consequence of this behavior is an *essential reduction* of the linear Rashba energy splitting $\Delta_R \propto k_y$, contrasting the expectation that the additional mechanism of the SO interaction should intensify the splitting rather than suppress it.

To understand the peculiarities of Fig. 3(b) we note that in Sec. II B it was shown that a finite β coupling leads to spatial separation between ''up'' and ''down'' spinor components (see Fig. 1). As a result, the orthogonality condition (34) no longer applies. Instead, the asymptotics (12)–(15) should be used. If we now calculate the Rashba splitting Δ_R (31), then we will see that scalar products $\langle \phi^n_{\uparrow\downarrow} | \phi^{n\pm1}_{\downarrow\uparrow} \rangle$ give nonzero (viz. linear in l_ω/l_β) contributions to the diagonal matrix elements $P^{nn}_{\uparrow\downarrow}$, so that Δ_R is now described by [cf. Eq. (35)]

$$\Delta_R \simeq 2\left[1-\left(n+\frac{1}{2}\right)\frac{l_\omega}{l_\beta}\right]\frac{l_\omega}{l_\alpha}(k_y l_\omega). \tag{42}$$

From this formula it immediately follows that the energy splitting Δ_R *diminishes* in comparison with Fig. 3(a) by an amount $(n+1/2)(l_\omega/l_\beta)$ that is *proportional* to the quantum level number n. This conclusion agrees well with data presented in Fig. 3(b).

The result (42) can be interpreted in the language of interstate coupling. Actually, it is easy to verify that the asymptotics (12)–(15) give rise to an additional (proportional to l_ω/l_β) term $\delta\Phi^n_\beta(t)$ in the wave function correction $\delta\Phi^n_{\uparrow\downarrow}(t)$ (37):

$$\begin{aligned}\delta\Phi^n_\beta(t) \simeq \frac{1}{2}\frac{l_\omega}{l_\alpha}\frac{l_\omega}{l_\beta}(k_y l_\omega)\Bigg[&\pm\sqrt{\frac{n+1}{2}}(k_y l_\omega)\,\phi^{n+1}_{\uparrow\downarrow}(t) \\ &\mp\sqrt{\frac{n}{2}}(k_y l_\omega)\,\phi^{n-1}_{\uparrow\downarrow}(t) \\ &+\frac{1}{4}\sqrt{(n+1)(n+2)}\,\phi^{n+2}_{\uparrow\downarrow}(t) \\ &-\frac{1}{4}\sqrt{n(n-1)}\,\phi^{n-2}_{\uparrow\downarrow}(t)\Bigg].\end{aligned} \tag{43}$$

This term, as well as $\delta\Phi^{n}_{\uparrow\downarrow}$ (37), involves ''nearest'' unperturbed wave functions $\phi^{n\pm1}_{\uparrow\downarrow}$. Since parameters l_ω/l_α and l_ω/l_β are independent of each other, we conclude that the β coupling enhances the hybridization between an nth and $(n\pm1)$-st electron states and thereby the anticrossing of corresponding energy branches. The strength of the hybridization grows with the growth of n.

Because of the enhanced interstate coupling, the anticrossing of neighboring energy branches in Fig. 3(b) is not restricted to a narrow region of relatively small values of $k_y l_\omega \lesssim 5$ as it was in Fig. 3(a). Instead, we can see that for all $n>0$ there exists a second anticrossing in the region $k_y l_\omega \approx 7-10$. Moreover, for larger quantum numbers $n \geqslant 4$ a third anticrossing emerges at $k_y l_\omega \approx 13-14$.

D. Ballistic conductance

To apply the results of the previous subsections to the study of the effect of the SO interaction on the ballistic conductance of a long Q1DES at low temperature, we must relate its conductance to its energy spectrum. Here we do this using the two-probe Landauer formula[46]

$$G \equiv G(\varepsilon_F) = \frac{e^2}{h} M(\varepsilon_F), \tag{44}$$

where G is the ballistic conductance, ε_F is the Fermi energy, and $M(\varepsilon_F)$ is the number of occupied electron subbands which propagate in the same direction:

$$M(\varepsilon_F) = \sum_n \sum_i \sum_{s=\uparrow,\downarrow} \theta[\varepsilon_F - \varepsilon^s_{min}(n,i)]. \tag{45}$$

Here $\varepsilon^s_{min}(n,i)$ is the energy of the ith minimum in the nth electron subband with the spin orientation s. $\theta(x)$ is the Heaviside unit step function. As will be seen later, the SO interaction can produce multiple minima in each 1D subband owing to the anticrossings between different subbands. Since $\varepsilon^s_{min}(n,i)$ can be found directly from the dispersion law of electrons, the conductance G (44) turns out to be *completely defined* by the energy spectrum alone. Therefore, as long as the expression (44) applies, the knowledge of the electron energy levels in a Q1DES will be sufficient to predict the behavior of the ballistic conductance as a function of the Fermi energy.

The applicability of Eq. (44), as well as of the general scattering approach[46] to quantum transport, is essentially based on the condition that a current must travel in any 1D electron subband without scattering into any other. In Ref. 47 it was shown that this *current conservation* condition holds true in quite general circumstances including placing a Q1DES in both a finite external magnetic field and an arbitrary external electrostatic potential. However, the proof in Ref. 47 ignored spin degrees of freedom and therefore did not take into account potentials acting in the spin space. Such neglect is not valid for our problem where the SO interaction Hamiltonian (1) leads to a highly nontrivial role for the spin in forming the energy spectrum of electrons (see Sec. II A–II C). For that reason we cannot rely on the conclusion of Ref. 47 but should check explicitly if the current is still conserved in the presence of a finite SO coupling.

The first step is to define the matrix elements of the current density $\mathbf{j}_{mn}(\mathbf{r})$ for the case where the wave functions $\Psi_{m(n)}(\mathbf{r})$ are spinors,[10] $\Psi_{m(n)} = \{\Psi^{m(n)}_{\uparrow}, \Psi^{m(n)}_{\downarrow}\}$:

$$\mathbf{j}_{mn}(\mathbf{r}) = \frac{1}{2M}\{\Psi^\dagger_m \hat{\boldsymbol{\sigma}}(\hat{\boldsymbol{\sigma}}\cdot\hat{\mathbf{p}})\Psi_n + [(\hat{\boldsymbol{\sigma}}\cdot\hat{\mathbf{p}})\Psi_m]^\dagger \hat{\boldsymbol{\sigma}}\Psi_n\}. \tag{46}$$

Here, the dagger denotes the Hermitian conjugate and $\hat{\mathbf{p}} = -i\hbar\nabla$. It is straightforward to verify that the divergence of the vector $\mathbf{j}_{mn}(\mathbf{r})$ is given by

$$\nabla\cdot\mathbf{j}_{mn}(\mathbf{r}) = \frac{i\hbar}{2M}\{(\nabla^2\Psi^\dagger_m)\Psi_n - \Psi^\dagger_m(\nabla^2\Psi_n)\}. \tag{47}$$

We now suppose that the Hamiltonian of the system has the general form $\hat{H} = \hat{\mathbf{p}}^2/2M + \hat{Q}$, where $\hat{Q}$ is a Hermitian operator ($\hat{Q}^\dagger = \hat{Q}$) that acts in both coordinate and spin spaces. As applied to our problem, $\hat{Q} = V_{LC} + \hat{H}_{SO}$ [see Eq. (2)]. Using this Hamiltonian and the Schrödinger equation $\hat{H}\Psi = E\Psi$, we express $\nabla^2\Psi^\dagger_m$ and $\nabla^2\Psi_n$ in terms of $\Psi^\dagger_m$ and Ψ_n, respectively, and substitute the expressions obtained into Eq. (47). As a result, we have

$$\nabla\cdot\mathbf{j}_{mn}(\mathbf{r}) = \frac{i}{\hbar}(E_m - E_n)\Psi^\dagger_m(\mathbf{r})\Psi_n(\mathbf{r}), \tag{48}$$

where E_m and E_n are energies corresponding to the states Ψ_m and Ψ_n, respectively. In the absence of any inelastic collisions, any scattering occurs between states of the same energy. So, without loss of generality, we can restrict ourselves to considering only equal energies $E_m = E_n$ in Eq. (48), in which case we find that

$$\nabla\cdot\mathbf{j}_{mn}(\mathbf{r}) = 0 \quad \text{for} \quad E_m = E_n. \tag{49}$$

This fundamental identity ensures *local* current conservation in the system. Once it has been established, if the system is translationally invariant in the longitudinal direction, further steps in proving the *global* conservation of current do not depend on specifics of the Hamiltonian and can be carried out in line with Ref. 47. Therefore, we arrive at the conclusion that the total current (i.e., current integrated over the cross section of the channel) between states m and n at $E_m = E_n$ is equal to zero unless $m=n$. In other words, eigenstates of the Hamiltonian $\hat{H}$ are perfect current-carrying states that are free from scattering even in the presence of arbitrary SO coupling.

For our problem, this result implies that the spectrum of the Hamiltonian (2) is directly relevant to and completely defines the ballistic conductance in the presence of the SO coupling. This allows us to use the simple Landauer formula (44), (45), in which the minima $\varepsilon^s_{min}(n,i)$ of the energy subbands can be found from the analysis of the spectrum presented in Secs. II A–II C.

Now we are in a position to discuss the features of the ballistic conductance in a Q1DES subject to the SO interaction. For illustrative purposes, we start with the ''ideal'' case of zero SO coupling. The corresponding subband energies $\varepsilon(n) = 2n + 1 + (k_y l_\omega)^2$ are plotted in Fig. 5(a) (solid curves) as functions of $k_y l_\omega$. The dependence $G(\varepsilon_F)$ can simply be deduced from this figure by moving a horizontal line ε

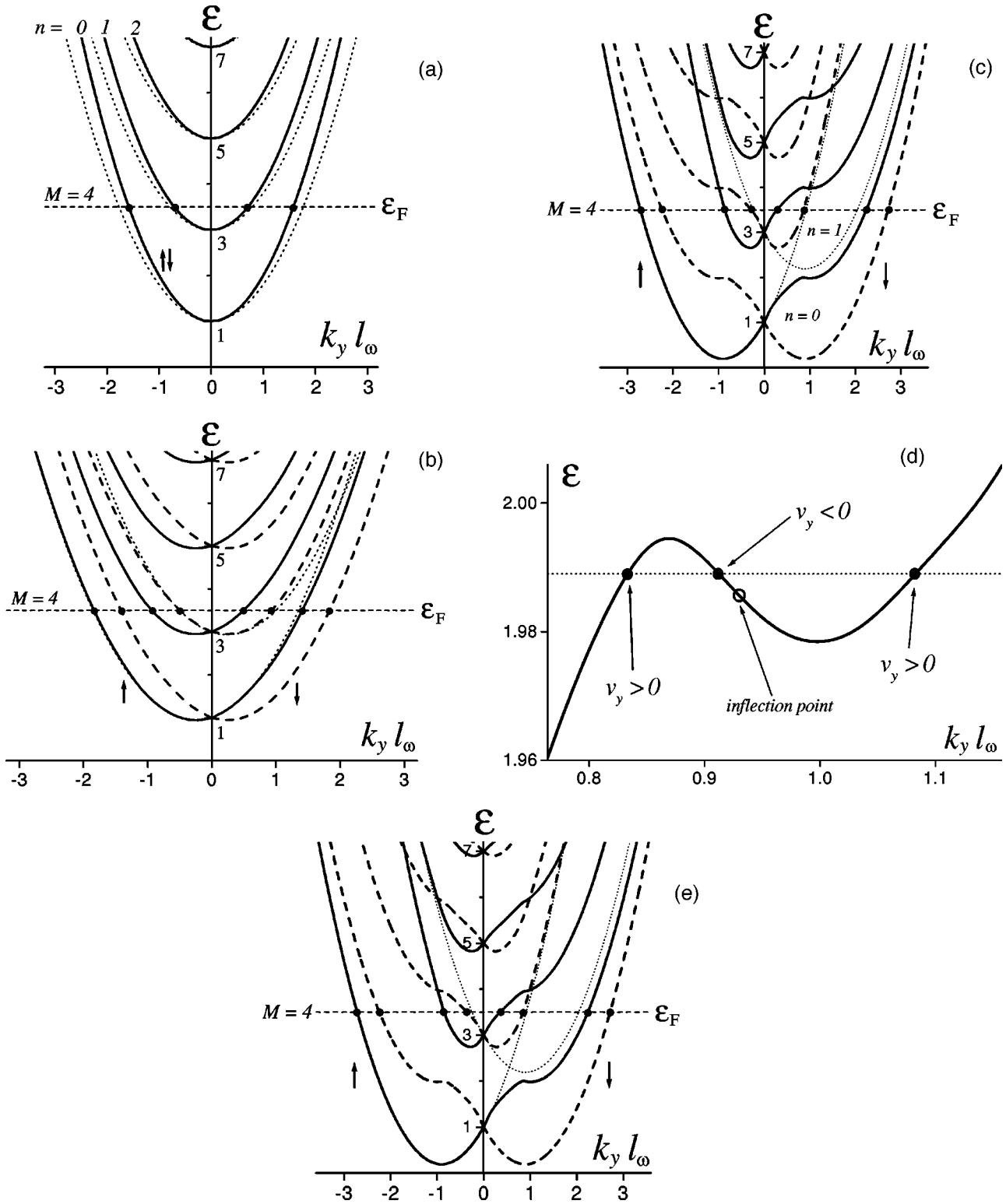

FIG. 5. The subband energy ε in units of $\hbar\omega/2$ vs $k_y l_\omega$: (a) zero SO coupling (solid curves), finite β coupling (dotted curves); (b) weak α coupling ($l_\omega/l_\alpha < \sqrt{2}$); (c) strong α coupling ($l_\omega/l_\alpha > \sqrt{2}$) and zero β coupling; (d) a magnified bump on an $n=0$ energy branch in the anticrossing region; (e) strong α coupling ($l_\omega/l_\alpha > \sqrt{2}$) and finite β coupling.

$=\varepsilon_F$ from zero upwards and counting the number of points at which this line crosses the spectral parabolas. Since all the subbands in an ideal system are twofold spin degenerate for any k_y, this number coincides with the number M of propagating modes in the Q1DES. As a result, we restore the well-known picture[2–5,9] of ballistic conductance quantization with equidistant jumps, each of height $2e^2/h$ [solid curve in Fig. 6(a)].

Dotted curves in Fig. 5(a) show subband energies $\varepsilon(n) = \varepsilon_x^{(0)}(n) + (k_y l_\omega)^2$ in the presence of the β coupling [see Eq. (16)]. Each subband is twofold spin degenerate. It is seen that for any given value of ε_F the number M of forward

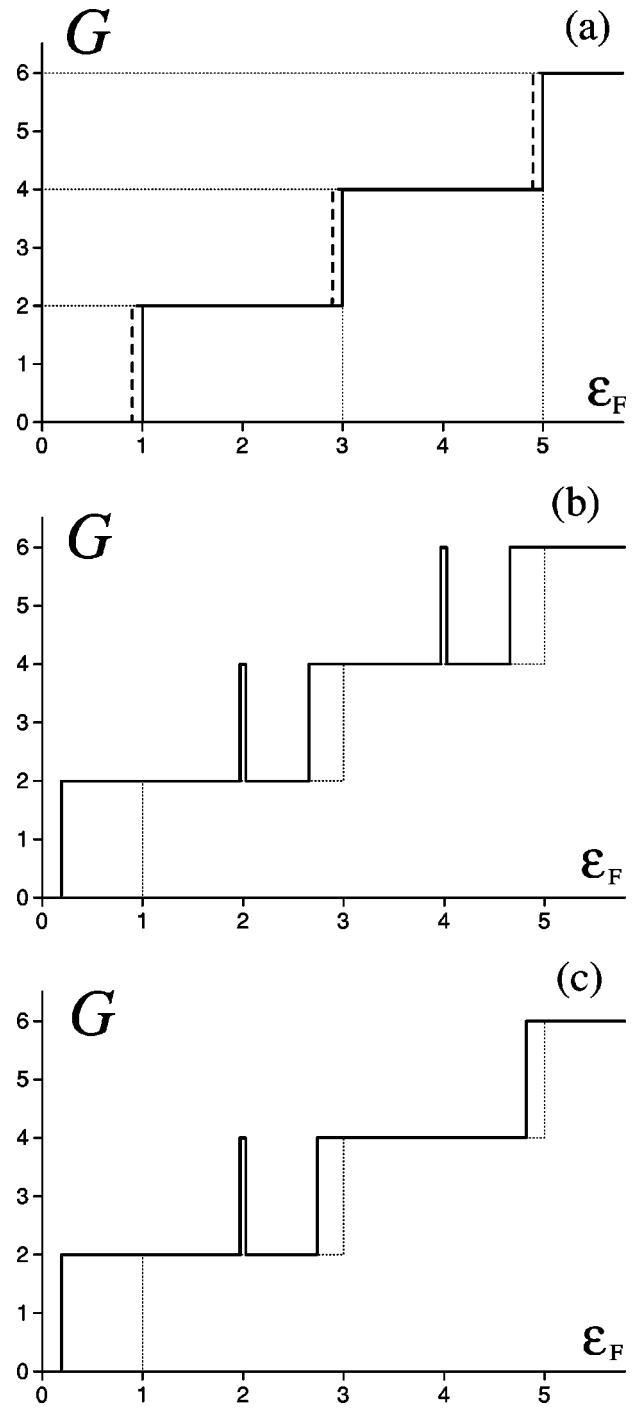

FIG. 6. The conductance G in units of e^2/h vs the Fermi energy ε_F in units of $\hbar\omega/2$: (a) zero SO coupling and finite β coupling (solid line), weak α coupling (dashed line); (b) strong α coupling and zero β coupling; (c) strong α coupling and finite β coupling.

propagating modes remains the same as it was in the ideal limit. Thus, we conclude that the β coupling alone does *not* affect the ballistic conductance. To detect the presence of the β coupling in a system, one should exploit a unique feature that can only be due to the β coupling. As a reasonable example of such a feature, we mention the spatial separation between spinor components that was established in Sec. II B and illustrated in Fig. 1. Owing to this effect, the regions of the most probable distribution of electrons with opposite spin orientations will be shifted apart in the transverse direction. By analogy with ferromagnetic materials, this effect can manifest itself in the appearance of the magnetization of the electron system and its dependence on the transverse coordinate.

Now we move on to the more complex case of finite α coupling. To start with, let us imagine the fictitious situation where the linear Rashba energy splitting

$$\Delta_R = 2(l_\omega/l_\alpha)(k_y l_\omega)$$

[see Eq. (35) and Fig. 3(a)] holds true not only for small values of $k_y l_\omega$ but for all $k_y l_\omega$. Here, the subband energies would be given by $\tilde{\varepsilon}_{\uparrow\downarrow}(n) = 2n+1+(k_y l_\omega)^2 \pm (l_\omega/l_\alpha)(k_y l_\omega)$. This formula describes parabolas of the same form as the solid curves in Fig. 5(a) but shifted by an amount $\pm(1/2)(l_\omega/l_\alpha)$ along the abscissa and lowered vertically by $(1/4)(l_\omega/l_\alpha)^2$. The parabolas $\tilde{\varepsilon}_{\uparrow\downarrow}(n)$ were used in Ref. 35 to predict spontaneous spin polarization of ballistic electrons in quantum wires due to spin splitting. Whereas the *real* energy branches $\varepsilon_\uparrow(n)$ and $\varepsilon_\downarrow(n+1)$ anticross [see Fig. 3(a)], the fictitious dispersion curves $\tilde{\varepsilon}_\uparrow(n)$ and $\tilde{\varepsilon}_\downarrow(n+1)$ *cross* at the point $k_y l_\omega = (l_\omega/l_\alpha)^{-1}$. This point remains the same for all numbers n and goes to infinity as the SO coupling vanishes. It is easy to verify that for $l_\omega/l_\alpha < \sqrt{2}$, the crossing point $k_y l_\omega = (l_\omega/l_\alpha)^{-1}$ lies to the right of the point $k_y l_\omega = (1/2)(l_\omega/l_\alpha)$ at which the parabola $\tilde{\varepsilon}_\downarrow(n+1)$ has the minimum. At the same time, if $l_\omega/l_\alpha > \sqrt{2}$, then the crossing point turns out to be to the left of the minimum point. Below we will see that these simple conclusions following from the *fictitious* energy spectrum play an important role in determining the behavior of the conductance $G(\varepsilon_F)$.

Figure 5(b) presents the energy subbands $\varepsilon_{\uparrow\downarrow}(n)$ (solid and dashed curves) of a Q1DES in the case of *weak* α coupling when $l_\omega/l_\alpha < \sqrt{2}$ (more specifically, $l_\omega/l_\alpha = 0.5$). Dotted lines indicate the *fictitious* energy levels $\tilde{\varepsilon}_\uparrow(n=0)$ and $\tilde{\varepsilon}_\downarrow(n=1)$. In full accordance with the above conclusions, these levels cross to the *right* of the bottom of the parabola $\tilde{\varepsilon}_\downarrow(n=1)$. As a result, the crossing angle turns out to be quite small. From Fig. 5(b) it is seen that this angle determines essentially the shape of the *real* energy curves $\varepsilon_\uparrow(n=0)$ and $\varepsilon_\downarrow(n=1)$ within the anticrossing region $1.5 \lesssim k_y l_\omega \lesssim 3$. As long as the angle is small, the anticrossing remains very smooth and the curves $\varepsilon_\uparrow(n=0)$ and $\varepsilon_\downarrow(n=1)$ behave very much like the ideal parabolas in Fig. 5(a). The same observation is also true for higher quantum numbers n. Such similarity suggests that weak α coupling $(l_\omega/l_\alpha < \sqrt{2})$ does not have a strong effect on the conductance. Indeed, it is easy to see by scanning Fig. 5(b) with the horizontal line $\varepsilon = \varepsilon_F$, that the only effect of weak α coupling on $G(\varepsilon_F)$ is to shift the conductance quantization steps down to lower energies by an amount $(1/4)(l_\omega/l_\alpha)^2$ [see dashed lines in Fig. 6(a)].

As soon as the coupling constant l_ω/l_α gets over the threshold of $\sqrt{2}$, the spectral picture becomes much more interesting. Figure 5(c) shows a case when $l_\omega/l_\alpha = 1.8$. Here the parabolas $\tilde{\varepsilon}_\uparrow(n=0)$ and $\tilde{\varepsilon}_\downarrow(n=1)$ (dotted curves) cross to the *left* of the bottom of $\tilde{\varepsilon}_\downarrow(n+1)$, which makes the crossing angle relatively large. The direct consequence of this is that the energy branches $\varepsilon_\uparrow(n=0)$ and $\varepsilon_\downarrow(n=1)$ cannot now

anticross as smoothly as they did for $l_\omega/l_\alpha<\sqrt{2}$. Instead, in order to keep continuity, the lower curve [i.e., $\varepsilon_\uparrow(n=0)$] is forced to exhibit a nonmonotonic portion (''bump'') within the anticrossing region. Although the height of the bump is rather small (~ 0.05 in the dimensionless units or ~ 0.25 meV as determined from typical subband spacings[48]), its geometry is a unique feature of the SO coupling mechanism [see a magnified plot of the bump in Fig. 5(d)]. The remarkable fact about it is that the bump contains a region where the electron energy decreases as the wave number grows. In other words, there exists an energy interval within which electrons are allowed to have a negative longitudinal group velocity $v_y=\hbar^{-1}(\partial\varepsilon/\partial k_y)<0$ for positive k_y. Since this interval has a finite width and is surrounded by energy domains with positive group velocities, the curvature of the line $\varepsilon=\varepsilon(k_y)$ reverses sign within the negative-velocity interval and therefore there exists an inflection point where $\partial^2\varepsilon/\partial k_y^2=0$ [see Fig. 5(d)]. At this point the effective electron mass $M=\hbar^2(\partial^2\varepsilon/\partial k_y^2)^{-1}$ diverges. Since the current passing through a 1D subband is proportional to the product of the group velocity and the density of states,[3,9] the singular effective mass has no effect on the conductance in the absence of electron scattering. However, it could significantly change the dependence $G(\varepsilon_F)$ in the presence of a scattering mechanism (e.g., disorder or electron-electron interaction).

As far as transport through 1D electron subbands is concerned, it is clear from Fig. 5(d) that the negative propagating mode coexists with a forward propagating mode with the same spatial wave function. In this physical situation it is likely that weak elastic scattering between these states would result in directed localization[49] so that they would not be observed in conductance.

However, if both forward and backward electron modes contribute equally to the conductance, then this immediately brings us to the conclusion that the bump on the curve $\varepsilon_\uparrow(n=0)$ gives rise to a peak in the dependence $G(\varepsilon_F)$ [see Fig. 6(b)]. The height of the peak is $2e^2/h$ and its width is defined by the height of the bump. Analogous bumps can be observed for all quantum levels $n=0,1,2,\ldots$. As a consequence, the sharp peak is seen in Fig. 6(b) not only on the first conductance plateau $G=2e^2/h$ but also on the second one $G=4e^2/h$ and would still be seen on all further plateaus.

Of course, the strong α coupling ($l_\omega/l_\alpha>\sqrt{2}$), as well as the weak coupling ($l_\omega/l_\alpha<\sqrt{2}$), shifts the conductance quantization steps to lower values of the Fermi energy in comparison with the ideal situation where $l_\omega/l_\alpha=0$. However, in contrast to the weak-coupling limit, strong coupling makes this shift much larger for the first step than for the others. This effect is clearly seen in Fig. 6(b) as opposed to the ideal conductance quantization shown by dotted lines. The larger shift of the first step is explained by the fact that the $n=0$ quantum state does not have a neighbor with the next lowest quantum number n. The energy level $\varepsilon_\downarrow(n=0)$ is therefore not forced to anticross with any other (lower lying) energy branch and therefore nothing affects its linear (Rashba) dependence on k_y [see Fig. 3(a)].

The final step of our analysis is to consider the case where both strong α coupling ($l_\omega/l_\alpha=1.8$) and relatively weak β coupling ($l_\omega/l_\beta=0.2$) are present in the system. The corresponding energy bands are shown in Fig. 5(e). As we demonstrated in Sec. II C, finite β coupling tends to suppress the energy splitting caused by the α coupling [cf. Figs. 3(a) and 3(b) and see Eq. (42)]. Effectively, this suppression can be interpreted as the enhancement of the anticrossing between neighboring energy branches $\varepsilon_\uparrow(n)$ and $\varepsilon_\downarrow(n+1)$. In Fig. 5(e) this effect is seen as a decrease in the gap between energy branches $\varepsilon_\uparrow(n)$ and $\varepsilon_\downarrow(n)$ ($n=1,2,3,\ldots$) in comparison with Fig. 5(c). Moreover, in accordance with Eq. (42), the gap becomes monotonically smaller as n grows. The enhanced anticrossing has a drastic effect on the energy bumps created by the strong α coupling: all the bumps except for the lowest one are now smoothed away and do not give rise to the two additional (forward and backward) propagating modes. As a result, the conductance exhibits only one sharp peak that occurs on the plateau $G=2e^2/h$ [see Fig. 6(c)]. A second effect of the enhanced anticrossing on the conductance is that the conductance quantization steps (starting from the second one) are now located closer to the ideal steps than they were for zero β coupling. As each next step appears, its distance from the corresponding ideal step diminishes until eventually they fuse.

There is another effect of the enhanced energy anticrossing on the conductance that is not seen in Figs. 6 but could possibly be detected in the presence of impurities. It is found experimentally[50,51] that the ballistic conductance quantization breaks down as the constriction becomes too long (at least $\gtrsim 2$ μm). This effect can be attributed to potential fluctuations caused by the random distributions of remote impurities. Zagoskin *et al.*[52] showed analytically that the degradation of quantized conductance decreases exponentially with the ratio of the 1D subband spacings to the standard deviation of impurity potential fluctuations. Obviously, the subband spacings depend on the presence of the SO interaction (see Figs. 5). By comparing Figs. 5(c) and 5(e) we see that a finite β coupling pushes neighboring energy branches apart and thus increases the subband spacings (possibly by tens of percent). This means that the presence of the β mechanism of the SO interaction could allow the experimental observation of the conductance quantization structure in longer samples.

III. CONCLUSION

We have studied theoretically the influence of the spin-orbit (SO) interaction on the energy spectrum and the ballistic conductance of a quasi-1D electron system (Q1DES) formed by lateral electric confinement of a 2D electron gas. The presence of the confining potential proves to be crucial in two ways. First, it alters significantly the effect of the quantum well asymmetry on the energy spectrum in comparison with a purely 2D system. As it was shown by Rashba *et al.*,[28,29] in 2D electron gases this asymmetry gives rise to SO coupling (which we refer to as the α coupling) that manifests itself in a lifting of the spin degeneracy of electronic states. The accompanying energy splitting Δ_R was found to be proportional to the in-plane electron wave number k. We have demonstrated that in a Q1DES the function $\Delta_R(k)$ is *nonmonotonic* [Fig. 3(a)] with the standard linear dependence[28,29] $\Delta_R\propto k$ being observed for relatively small and large values of k only. Such a drastic change in behavior is explained by the essentially different effect of SO coupling

operator $\hat{P}_{\uparrow\downarrow}$ (33) on unperturbed wave functions depending on whether or not the lateral confining potential is taken into account. Indeed, in the zero-potential case the unperturbed wave functions are plane waves characterized by the continuous in-plane wave vector **k** and the spin. The action of the operator $\hat{P}_{\uparrow\downarrow}$ on any such wave function reduces to a simple renormalization of its amplitude with the renormalizing factor being independent of coordinates. As a consequence of this simple effect, wave functions belonging to different values of **k** remain independent of each other and the SO coupling manifests itself in linear (monotonic) energy splitting $\Delta_R \propto k$ which is the same for all quantum states.

In contrast to this, the wave functions in the presence of a finite confining potential have a more complicated structure (10) and are characterized by the discrete quantum number n instead of the continuous transverse wave number. According to Eq. (20), the action of the operator $\hat{P}_{\uparrow\downarrow}$ on the nth wave function includes projecting it onto states with the next (preceding) closest quantum numbers $n\pm1$. In turn, the $(n\pm1)$-st states are projected onto their ''neighbors'' with numbers n and $n\pm2$, respectively. As a result, the operator $\hat{P}_{\uparrow\downarrow}$ *couples* effectively any nth and $(n\pm1)$-st wave functions. In other words, once the SO coupling has been taken into account, the nth and $(n\pm1)$-st wave functions cease to be independent and possess symmetry elements of each other. This partial symmetry between states leads to an *anticrossing* of the closest (neighboring) energy branches in Fig. 3(a) and hence to the nonmonotonic dependence $\Delta_R(k)$.

Apart from the interplay with the familiar (quantum-well-asymmetry or Rashba) mechanism of the SO interaction, the lateral confining potential by itself appears to be a source of additional dynamical coupling between the orbital and spin degrees of freedom of an electron. This coupling (which we refer to as β coupling) originates from the natural spatial nonuniformness of the confining potential. A typical variation scale of this potential lies within the wide range $\sim 10-1000$ nm, which makes the accompanying electric field sufficiently strong to compete with the quantum-well-asymmetry field. This competition may become especially noticeable in square quantum wells with a relatively weak Rashba contribution. Whereas the quantum-well field is normal to the device plane, the confinement-induced electric field is parallel to the plane. It is also spatially nonuniform as long as the coordinate dependence of the confining potential is more complex than linear. These features make the β coupling an essentially different mechanism of the SO interaction in a Q1DES which *cannot* be taken into account by simply adjusting the Rashba interaction constant. This claim is confirmed by Fig. 3(b) which demonstrates the combined effect of both the Rashba and the confinement-induced couplings on the energy spectrum. From comparison of Fig. 3(b) with Fig. 3(a) we see that the major role of β coupling is to *reduce* the Rashba energy splitting Δ_R (see region $k_y l_\omega \lesssim 2$) rather than to give a positive correction to it. It is crucial that the reduction depends on the quantum number n and monotonically grows as n increases. This fact is a clear manifestation of the position dependence of the electric field created by the confining potential and indicates the independent nature of β coupling. The suppression of the Rashba energy splitting is a part of the overall effect of the β coupling on the underlying electron system which consists of a considerable enhancement of the hybridization between different quantum states and eventually leads to a more pronounced anticrossing of neighboring energy branches.

In addition to the investigation of the SO effects in the energy spectrum of electrons, we have discussed the possible manifestations of the SO interaction in the ballistic conductance of a Q1DES. The key point of our approach to the conductance is the fundamental *current-conservation identity* that was proven in Sec. II D. According to this identity, the electron eigenstates that were found as the solution to the spectral problem are *perfect* current-carrying states. A current can travel in any of these states without scattering into any other. This property therefore allows the ballistic conductance to be calculated directly from the energy spectrum with the help of simple Landauer formula (44).

An analysis of the ballistic conductance G reveals that the β coupling alone does *not* affect the dependence of G on the Fermi energy ε_F. This fact is illustrated by Fig. 5(a) where we see that the β coupling reduces the curvature of the parabolic energy bands (cf. dotted and solid curves), while the band edges (bottoms of the parabolas) remain anchored. Thus, β coupling cannot be detected by measuring the ballistic conductance in systems where the SO interaction appears *only* in a form of the β coupling (e.g., in square wells). Instead, one should use experimental methods that allow direct observation of the electron energy spectrum in a Q1DES, e.g., magnetotunneling measurements.[40]

In the presence of α coupling, the behavior of $G(\varepsilon_F)$ is essentially determined by the strength of the SO interaction. If the α coupling is not too strong $(l_\omega/l_\alpha < \sqrt{2})$, then its only effect on the conductance will be shifts of the conductance quantization steps to lower Fermi energies in comparison with an ideal (i.e., with zero SO interaction) situation. We note that such shifts are not related to the lateral confining potential and should also be present in purely 2D systems. This effect should be detectable in transconductance measurements (see, e.g., Ref. 53) which determine both the conductance and the subband spacings simultaneously.

In the limit of strong α coupling $(l_\omega/l_\alpha > \sqrt{2})$ the electron energy bands take on a very interesting form [Fig. 5(c)]. The most remarkable feature is the appearance of narrow energy intervals where two additional (forward and backward propagating) electron modes exist [Fig. 5(d)]. Such intervals can be found in each 1D subband, starting from the lowest one. The additional electron modes have similar magnitude group velocities but propagate in opposite directions. They have almost identical subband wave functions and therefore would be susceptible to strong intermode scattering in the presence of disorder. However, in a sufficiently pure Q1DES, the additional electron modes give rise to the unusual periodic sharp steps in $G(\varepsilon_F)$ shown in Fig. 6(b). This picture is changed by switching on relatively weak $(l_\omega/l_\beta \ll l_\omega/l_\alpha)$ β coupling. As we mentioned above in the discussion of the energy spectrum, the β coupling enhances the anticrossing of energy levels initiated by the α coupling. As applied to the conductance, this effect leads to *quenching* the sharp conductance peaks by the β coupling. The existence of the single peak (or just a few of peaks) in the dependence of G on ε_F could be a clear experimental indication of the presence of the β coupling in the system.

The most crucial point for the experimental observation of the conductance peaks in Fig. 6 is to make the ratio l_ω/l_α sufficiently large ($l_\omega/l_\alpha > \sqrt{2}$). In typical systems, where enhancing the SO interaction is not paid special attention, the value of l_ω/l_α hardly exceeds 0.5. An additional, at least threefold, increase in l_ω/l_α could be achieved by using: (i) materials with light carrier masses; (ii) strong (narrow) lateral potential confinement $\lesssim 100$ nm; (iii) heterojunctions (triangular well) rather than quantum-well heterostructures (square well); (iv) a back gate voltage to maximize the interface (Rashba) electric field.

We hope that the results presented in this paper will stimulate further experimental and theoretical work with the aim of understanding the role of the spin-orbit interaction in determining the transport properties of quasi-1D systems.

ACKNOWLEDGMENTS

A.V.M. thanks the ORS, Cambridge Overseas Trust, and Corpus Christi College for financial support. C.H.W.B. thanks the EPSRC for support. This work was funded by the EPSRC.

[1] T. J. Thornton, M. Pepper, H. Ahmed, D. Andrews, and G. J. Davies, Phys. Rev. Lett. **56**, 1198 (1986).
[2] C. W. J. Beenakker and H. van Houten, *Quantum Transport in Semiconductor Nanostructures*, Solid State Physics Vol. 44 (Academic Press, New York, 1991).
[3] M. J. Kelly, *Low-Dimensional Semiconductors: Material, Physics, Technology, Devices* (Oxford University Press, Oxford, 1995).
[4] B. J. van Wees, H. van Houten, C. W. J. Beenakker, J. G. Williamson, L. P. Kouwenhoven, D. van der Marel, and C. T. Foxon, Phys. Rev. Lett. **60**, 848 (1988).
[5] D. A. Wharam, T. J. Thornton, R. Newbury, M. Pepper, H. Ahmed, J. E. F. Frost, D. G. Hasko, D. C. Peacock, D. A. Ritchie, and G. A. C. Jones, J. Phys. C **21**, L209 (1988).
[6] K. J. Thomas, J. T. Nicholls, M. Y. Simmons, M. Pepper, D. R. Mace, and D. A. Ritchie, Phys. Rev. Lett. **77**, 135 (1996).
[7] A. Kristensen, J. Bo Jensen, M. Zaffalon, C. B. Sørensen, S. M. Reimann, M. Michel, and A. Forchel, J. Appl. Phys. **83**, 607 (1998).
[8] K. J. Thomas, J. T. Nicholls, N. J. Appleyard, M. Y. Simmons, M. Pepper, D. R. Mace, W. R. Tribe, and D. A. Ritchie, Phys. Rev. B **58**, 4846 (1998).
[9] S. Datta, *Electronic Transport in Mesoscopic Systems* (Cambridge University Press, Cambridge, 1995).
[10] V. K. Thankappan, *Quantum Mechanics* (John Wiley & Sons, New York, 1993); L. I. Schiff, *Quantum Mechanics* (McGraw-Hill, New York, 1968).
[11] L. D. Landau and E. M. Lifshitz, *Quantum Mechanics* (Pergamon Press, Oxford, 1991).
[12] G. P. Fisher, Am. J. Phys. **39**, 1528 (1971).
[13] H. L. Stormer, Z. Schlesinger, A. Chang, D. C. Tsui, A. C. Gossard, and W. Wiegmann, Phys. Rev. Lett. **51**, 126 (1983).
[14] D. Stein, K. von Klitzing, and G. Weimann, Phys. Rev. Lett. **51**, 130 (1983).
[15] B. Das, D. C. Miller, S. Datta, R. Reifenberger, W. P. Hong, P. K. Bhattacharya, J. Singh, and M. Jaffe, Phys. Rev. B **39**, 1411 (1989).
[16] B. Das, S. Datta, and R. Reifenberger, Phys. Rev. B **41**, 8278 (1990).
[17] P. D. Dresselhaus, C. M. A. Papavassiliou, R. G. Wheeler, and R. N. Sacks, Phys. Rev. Lett. **68**, 106 (1992).
[18] B. Jusserand, D. Richards, H. Peric, and B. Etienne, Phys. Rev. Lett. **69**, 848 (1992).
[19] G. Goldoni and A. Fasolino, Phys. Rev. Lett. **69**, 2567 (1992).
[20] G. L. Chen, J. Han, T. T. Huang, S. Datta, and D. B. James, Phys. Rev. B **47**, 4084 (1993).
[21] J. Nitta, T. Akazaki, and H. Takayanagi, Phys. Rev. Lett. **78**, 1335 (1997).
[22] G. Dresselhaus, Phys. Rev. **100**, 580 (1955).
[23] J. Luo, H. Munekata, F. F. Fang, and P. J. Stiles, Phys. Rev. B **41**, 7685 (1990).
[24] R. Eppenga and M. F. H. Schuurmans, Phys. Rev. B **37**, 10 923 (1988).
[25] A. G. Mal'shukov, K. A. Chao, and M. Willander, Phys. Rev. Lett. **76**, 3794 (1996).
[26] V. M. Edelstein, J. Phys.: Condens. Matter **7**, 1 (1995).
[27] T. Ando, A. B. Fowler, and F. Stern, Rev. Mod. Phys. **54**, 437 (1982).
[28] E. I. Rashba, Fiz. Tverd. Tela (Leningrad) **2**, 1224 (1960) [Sov. Phys. Solid State **2**, 1109 (1960)].
[29] Yu. A. Bychkov and E. I. Rashba, Pis'ma Zh. Éksp. Teor. Fiz. **39**, 66 (1984) [JETP Lett. **39**, 78 (1984)].
[30] S. I. Dorozhkin and E. B. Ol'shanetskiĭ, Pis'ma Zh. Éksp. Teor. Fiz. **46**, 399 (1987) [JETP Lett. **46**, 502 (1987)].
[31] T. Hassenkam, S. Pedersen, K. Baklanov, A. Kristensen, C. B. Sorensen, P. E. Lindelof, F. G. Pikus, and G. E. Pikus, Phys. Rev. B **55**, 9298 (1997).
[32] A. Yacoby, H. L. Stormer, K. W. Baldwin, L. N. Pfeiffer, and K. W. West, Solid State Commun. **101**, 77 (1997); A. Yacoby, H. L. Stormer, N. S. Wingreen, L. N. Pfeiffer, K. W. Baldwin, and K. W. West, Phys. Rev. Lett. **77**, 4612 (1996).
[33] S. Datta and B. Das, Appl. Phys. Lett. **56**, 665 (1990).
[34] B. E. Kane, Nature (London) **393**, 133 (1998).
[35] G. Fasol and H. Sakaki, Phys. Rev. Lett. **70**, 3643 (1993); Appl. Phys. Lett. **62**, 2230 (1993).
[36] V. V. Kveder, Yu. A. Osip'yan, and A. I. Shalynin, Pis'ma Zh. Éksp. Teor. Fiz. **40**, 10 (1984) [JETP Lett. **40**, 729 (1984)]; V. V. Kveder, V. Ya. Kravchenko, T. R. Mchedlidze, Yu. A. Osip'yan, D. E. Khmel'nitskiĭ, and A. I. Shalynin, *ibid.* **43**, 202 (1986) [*ibid.* **43**, 255 (1986)].
[37] E. I. Rashba, Usp. Fiz. Nauk **84**, 557 (1964) [Sov. Phys. Usp. **7**, 823 (1965)].
[38] S. E. Laux, D. J. Frank, and F. Stern, Surf. Sci. **196**, 101 (1988).
[39] H. Drexler, W. Hansen, S. Manus, J. P. Kotthaus, M. Holland, and S. P. Beaumont, Phys. Rev. B **49**, 14 074 (1994).
[40] B. Kardynał, C. H. W. Barnes, E. H. Linfield, D. A. Ritchie, J. T. Nicholls, K. M. Brown, G. A. C. Jones, and M. Pepper, Phys. Rev. B **55**, R1966 (1997).
[41] G.-H. Chen and M. E. Raikh, Phys. Rev. B **60**, 4826 (1999).
[42] B. K. Ridley, *Quantum Processes in Semiconductors* (Clarendon Press, Oxford, 1993).
[43] G. E. Marques and L. J. Sham, Surf. Sci. **113**, 131 (1982).

[44] M. Abramowitz and I. A. Stegun, *Handbook of Mathematical Functions* (Dover Publications, New York, 1965).
[45] Yu. A. Bychkov, V. I. Mel'nikov, and E. I. Rashba, Zh. Éksp. Teor. Fiz. **98**, 717 (1990) [Sov. Phys. JETP **71**, 401 (1990)].
[46] R. Landauer, IBM J. Res. Dev. **1**, 253 (1957); R. Landauer, Philos. Mag. **21**, 863 (1970); R. Landauer, in *Localization, Interaction, and Transport Phenomena*, edited by G. Bergmann and Y. Bruynseraede (Springer-Verlag, New York, 1985).
[47] H. U. Baranger and A. D. Stone, Phys. Rev. B **40**, 8169 (1989).
[48] S. J. Koester, C. R. Bolognesi, M. Thomas, E. L. Hu, H. Kroemer, and M. J. Rooks, Phys. Rev. B **50**, 5710 (1994).
[49] C. Barnes, B. L. Johnson, and G. Kirczenow, Phys. Rev. Lett. **70**, 1159 (1993).
[50] G. Timp, R. Behringer, S. Sampere, J. E. Cunningham, and R. E. Howard, in *Proccedings of the International Symposium on Nanostructure Physics and Fabrication*, edited by M. A. Reed and W. P. Kirk (Academic, New York, 1989), p. 331.
[51] S. J. Koester, B. Brar, C. R. Bolognesi, E. J. Caine, A. Patlach, E. L. Hu, H. Kroemer, and M. J. Rooks, Phys. Rev. B **53**, 13 063 (1996).
[52] A. M. Zagoskin, S. N. Rashkeev, R. I. Shekhter, and G. Wendin, J. Phys.: Condens. Matter **7**, 6253 (1995).
[53] K. J. Thomas, M. Y. Simmons, D. R. Mace, M. Pepper, and D. A. Ritchie, Appl. Phys. Lett. **67**, 109 (1995).